SOLUTION MINING RESEARCH INSTITUTE
www.solutionmining.org

105 Apple Valley Circle
Clarks Summit, PA 18411, USA

Telephone: +1 570-585-8092

Technical Conference Paper

Salt-Fall Detection in Oil Storage Caverns

Pierre Bérest, LMS, Ecole Polytechnique, France
Benoît Brouard & Vassily Zakharov, Brouard Consulting, France
Dean Checkai, Fluor Federal Petroleum Operations, USA
David Hart, Sandia National Laboratories, USA

SMRI Fall 2017 Technical Conference
25 - 26 September 2017
Münster, Germany

Solution Mining Research Institute Fall 2017 Technical Conference
Münster, Germany, 25 - 26 September 2017

Salt-Fall Detection in Oil Storage Caverns

Pierre Bérest[1], Benoît Brouard[2], Dean Checkaï[3],
Hakim Gharbi[1], David Hart[4], Vassily Zakharov[2]

[1] Ecole Polytechnique, Palaiseau, France

[2] Brouard Consulting, Paris, France

[3] Fluor Federal Petroleum Operations, LLC, USA

[4] Sandia National Laboratories, Albuquerque, NM, USA

Sandia National Laboratories is a multi-mission laboratory managed and operated by National Technology and Engineering Solutions of Sandia LLC, a wholly owned subsidiary of Honeywell International Inc. for the U.S. Department of Energy's National Nuclear Security Administration under contract DE-NA0003525.

Abstract

In an oil-storage cavern, salt-block fall generates pressure waves that can be recorded at the brine-string wellhead. An example of this was provided in a paper presented during the Albuquerque SMRI Meeting by Hart et al. (2017). In the present paper, it is suggested that these pressure changes originate from gravity waves such that the brine-oil interface swings in the cavern. These events are easier to record when the brine-string shoe is not too far below the oil/brine interface (h_b on Figure 1) and when the offset between the brine-string shoe and the cavern axis of symmetry is sufficiently large (r_s on Figure 1). Information on block size can be inferred from the analysis of pressure waves.

Key words: Caverns for Oil storage, Cavern Testing, Waves in Salt Caverns, SPR, Big Hill.

Introduction

Salt falls are relatively frequent in salt caverns (Cole, 2002; Munson et al., 2004; Rokahr et al., 2007; Crotogino et al., 2001; Baar, 1977; Renoux et al., 2013). In some cases, strings are broken during the fall. At the SPR, a broken string due to a salt fall can be detected if the depth of break is above the oil-brine interface and the brine string fills with oil, thus increasing the pressure on the brine string. However, in many cases, these falls remain unobserved until they are revealed by a sonar survey or a gamma ray, performed several months or years after the fall, that detect shape change or bottom heave.

In natural gas caverns, sluffing and creep closure occur. The former generates no cavern volume change; however, both contribute to the raise of the gas-brine interface. Special methods allow discriminating between these two possible causes (Cole, 2002).

In oil-storage caverns, cavern pressure is higher than it is in gas caverns, and creep closure is slower. Several techniques can be used to detect salt falls in real time. The simplest consists of recording brine pressure (P_b) and oil pressure (P_o) at the wellhead accurately. When γ_o and γ_b are the volumetric weight of oil and brine, respectively, and *h* is the oil/brine interface depth:

$$P_o - P_b = (\gamma_b - \gamma_o) h \tag{1}$$

The exact values of γ_o and γ_b are not known *very accurately* (Typically, $\gamma_b = 0.012$ MPa/m $= 0.52$ psi/ft and $\gamma_o = 0.0085$ MPa/m $= 0.37$ psi/ft.), making any assessment of interface depth (h) uncertain. However, when comparing two *successive* positions of the interface, uncertainties are much smaller, $\delta(P_o - P_b) = (\gamma_b - \gamma_o)\delta h$, as volumetric weights remain constant. Consider, for instance, a cylindrical cavern whose diameter is 200 ft (60 m); its cross-sectional area is *S* = 31,000 ft^2 = 2800 m^2. A 1000 m^3-block falling from the upper part of the cavern generates an interface rise by $\delta h = 0.35$ m, or 1 ft, and a differential pressure change $\delta(P_o - P_b) = (0.52 - 0.37) \times 1 = 0.15$ psi ≈ 11 mbar, a value that is small but which can be detected easily when accurate pressure sensors are used.

Renoux et al. (2013) describe continuous digital microseismic monitoring performed since 1992 at Geosel-Manosque in France, where a 27-cavern oil storage is operated; 10,000 induced microseismic events with magnitude lower than 0.3 have been located within the storage perimeter. Some of them originate in block-fall events. Event location is of prime importance in this context as it allows a better understanding of cavern mechanical behavior.

In this paper, it is suggested that wellhead pressure evolution, when properly recorded at ground level, provides useful information on salt block falls.

Waves in a salt cavern

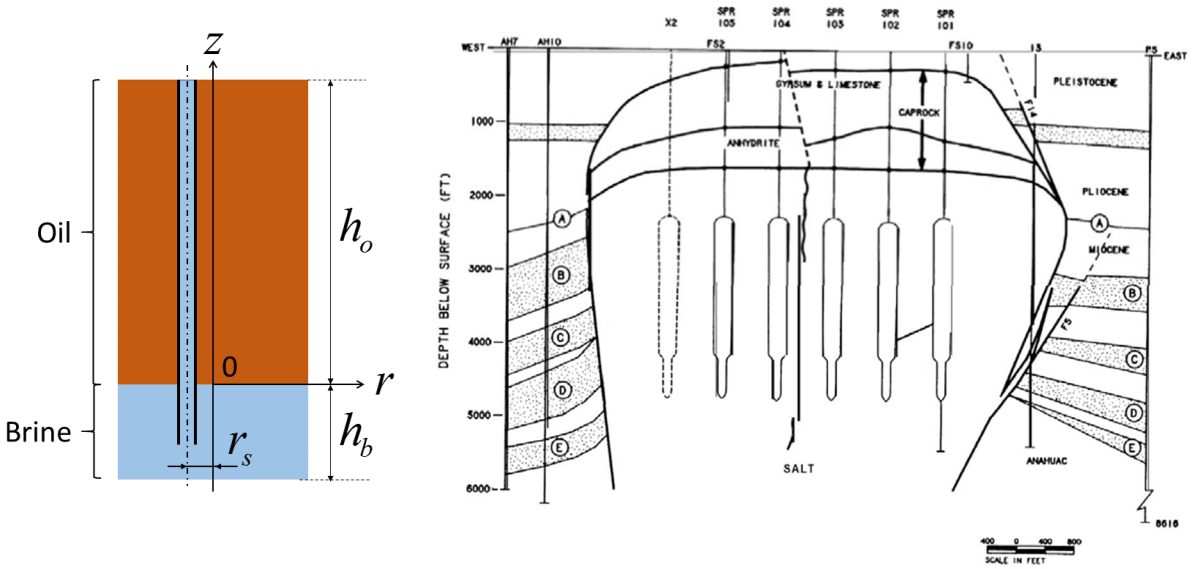

Figure 1 - The "box" (Park et al., 2005).

Many kinds of waves can be generated by pressure changes in a salt cavern (Bérest et al., 1999). Here, we are interested mainly in stationary waves (In the liquid body, the oscillation phase is the same at any point.) that develop some time after the transient waves that result from the initial pressure change vanish. These include the following.

- ***Quarter-waves in strings and annular spaces*** — Their period is $T = 4H/c$, where H is the distance from the wellhead to the tube (or annular space) shoe, and c is the velocity of sound in the string. The sound velocity in brine is $c = 1800$ m/s (5900 ft/s), but the sound velocity in a brine-filled string is slower, as the steel string is also somewhat compressible. When string thickness and stiffness are known, sound velocity in the string can be computed (or measured) easily. In a brine-filled string, it typically is $c = 3900$ ft/s (1200 m/s), and when the brine-string length is $H = 3900$ ft (1200 m), the quarter-wave period in the brine string is $T = 4$ seconds. In an oil-filled annulus, the velocity of sound is $c' = 3200$ ft/s (1000 m/s), typically; when the length of this annulus is 2200-ft (660 m), the quarter-wave period for this annulus is $T = 2.8$ seconds.

- ***Resonator's waves*** — These waves can be observed when the upper part of a string or an annulus is partially filled with gas (for instance, during an MIT). Their period depends on the gas-column height.

- ***Interface waves*** — They can be observed in a cavern containing an interface between two non-miscible fluids (e.g., oil and brine). Equilibrium demands that this interface be horizontal. When, following a perturbation, an interface departs from its horizontal equilibrium position, gravity forces tend to restore equilibrium. In sharp contrast with the waves described above, these waves do not result from fluid compressibility. Examples of such waves were described by Hart et al. (2017), who presented pressure records performed in BH112B (a brine well of a storage cavern at the Big Hill SPR site) following a salt fall (Figure 2):

> ''*The waveform from this particular salt fall event shows a maximum amplitude of ~80 PSI (0.55 MPa), a period of ten to twenty seconds, and evidence of two distinct underlying frequencies. The event lasts a total of ten minutes before decaying to within the noise limits of the compression algorithm.*'' (p. 14).

In the following, a tentative explanation of this phenomenon is proposed.

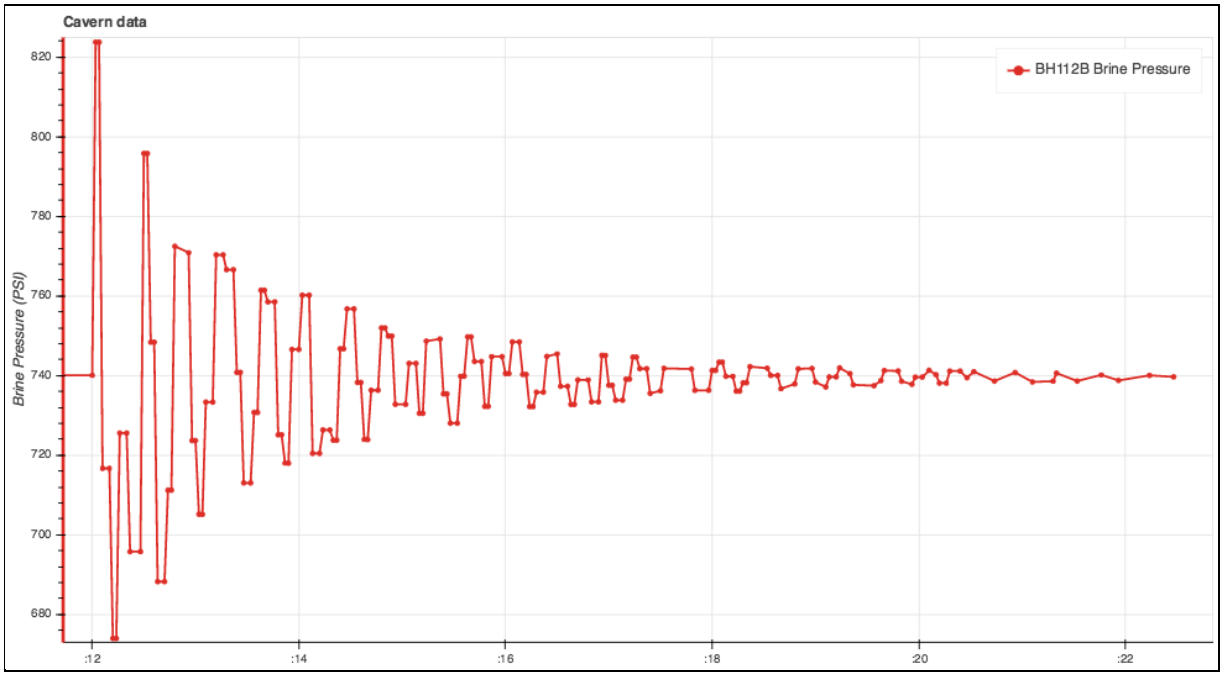

Figure 2 - Salt-fall event pressure signature at the wellhead, with time scale in minutes since 5:00 UTC (Hart et al., 2017).

Gravity Waves

A simple mathematical description of the gravity waves can be reached when considering a closed cylindrical "box" (see Figure 1). A mock-up test was performed also in a cylindrical glass vessel (Figure 3). To some extent, such a box mimics the elongated caverns of the Big Hill SPR site. It contains a heavy fluid (brine) and a light fluid (oil). At equilibrium, the interface coincides with the horizontal line $z = 0$. The depths of the cavern bottom and cavern roof are $z = -h_b$ and $z = h_o$, respectively. Both fluids are non-viscous (The role of viscosity will be discussed later.) and the momentum equation (Newton's equation) can be written as

$$\rho \frac{d\underline{v}}{dt} = -\underline{grad}\ p + \rho \underline{g} \tag{2}$$

Fluid compressibility is neglected: fluid density ρ is constant, $\rho = g/\gamma = \text{constant}$ and $\text{div}\, v = 0$, with g being gravity acceleration and v fluid velocity. In the acceleration term of the momentum equation, only the linear term is considered: $dv/dt \approx \partial v/\partial t$. When only stationary waves are considered, it can be inferred that there exist two harmonic ($\Delta\psi = 0$) functions, ψ_o and ψ_b, such that $\underline{v_o} = \cos\omega t\ \underline{grad}\ \underline{\psi_o}(r,\theta,z)$ and $\underline{v_b} = \cos\omega t\ \text{grad}\ \underline{\psi_b}(r,\theta,z)$. Pressure variations in oil and brine respectively are $p_o = -\gamma_o z - \frac{\gamma_o}{g}\frac{\partial \psi_o}{\partial t}$ and $p_b = -\gamma_b z - \frac{\gamma_b}{g}\frac{\partial \psi_b}{\partial t}$, where (r,θ) are polar coordinates.

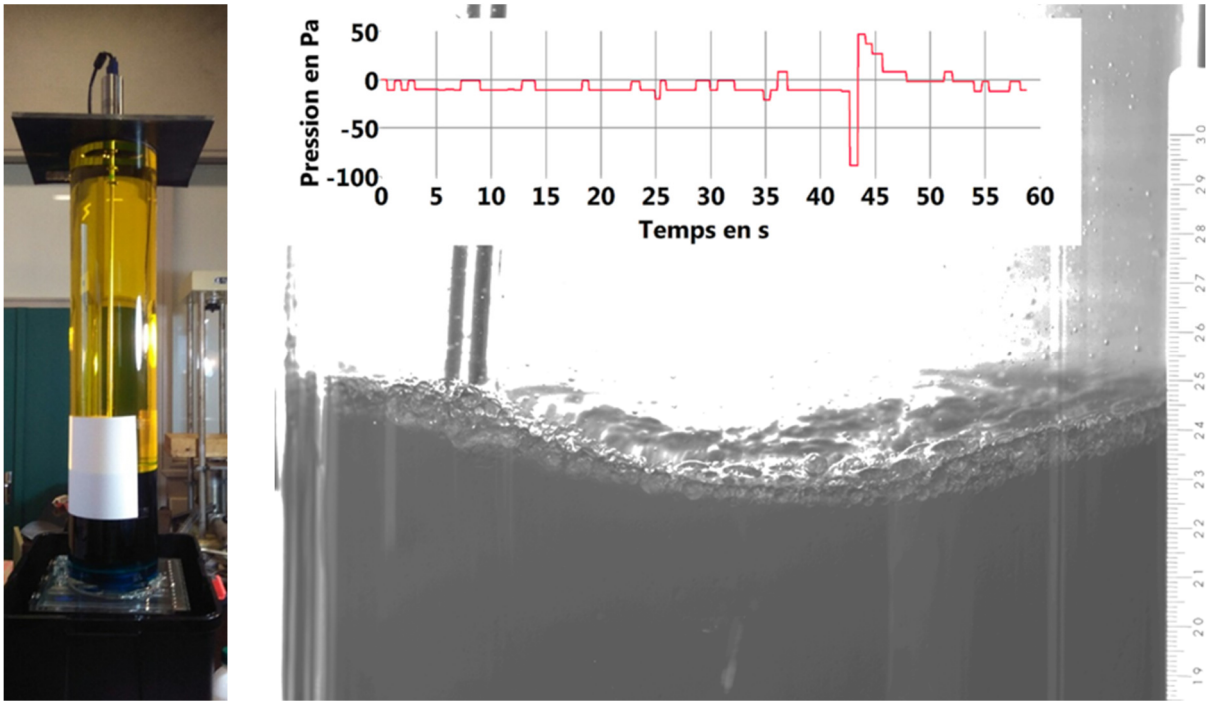

Figure 3 - A test was performed in a cylindrical glass vessel, diameter 20 cm (0.7 ft), height 1 m (3.3 ft). The fluids were kerdane and alcohol (90°). When a metallic ball drops in the vessel, at t = 42 s approximately, gravity waves are generated at the kerdane-alcohol interface.

Eigenmodes

Solutions of $\Delta\psi = 0$ satisfying the boundary conditions (fluid rate vanishing to zero at cavern walls, roof and bottom, and equal oil and brine rates at the brine-oil interface) can be written as a series of functions such that

$$\begin{cases} \psi_o(r,\theta,z) = \sum_{n,i} \psi_o^{n,i} = \sum_{n,i} C_{n,i}^o \cos(n\theta)\, J_n\left(\alpha_{n,i}\frac{r}{R}\right) \mathrm{ch}\left(\alpha_{n,i}\frac{z-h_o}{R}\right) \\ \psi_b(r,\theta,z) = \sum_{n,i} \psi_b^{n,i} = \sum_{n,i} C_{n,i}^b \cos(n\theta)\, J_n\left(\alpha_{n,i}\frac{r}{R}\right) \mathrm{ch}\left(\alpha_{n,i}\frac{z+h_b}{R}\right) \end{cases} \tag{3}$$

where $J_n(\alpha)$ is the *n*th Bessel function of the first kind, and $\alpha_{n,i}$ is the *i*th root of $dJ_n(\alpha)/d\alpha = 0$. In addition, pressure must be continuous through the oil-brine interface, leading to

$$\omega_{n,i}^2 = \frac{(\gamma_b - \gamma_o)g}{\alpha_{n,i}R\left[\gamma_b \coth\left(\alpha_{n,i}h_b/R\right) + \gamma_o \coth\left(\alpha_{n,i}h_o/R\right)\right]} \tag{4}$$

To each of these eigenvalues, $\omega_{n,i}$, is associated an eigenmode $\psi^{n,i}$, labelled (n,i). To each of these eigenmodes is associated a shape of the maximum vertical displacement of the interface. The shape of the interface displacement for the four eigenmodes whose periods ($T_{n,i} = 2\pi/\omega_{n,i}$) are longest are represented schematically on Figure 4. For each of these eigenmodes, one or several nodal lines can be defined. (There is no interface displacement along a nodal line.)

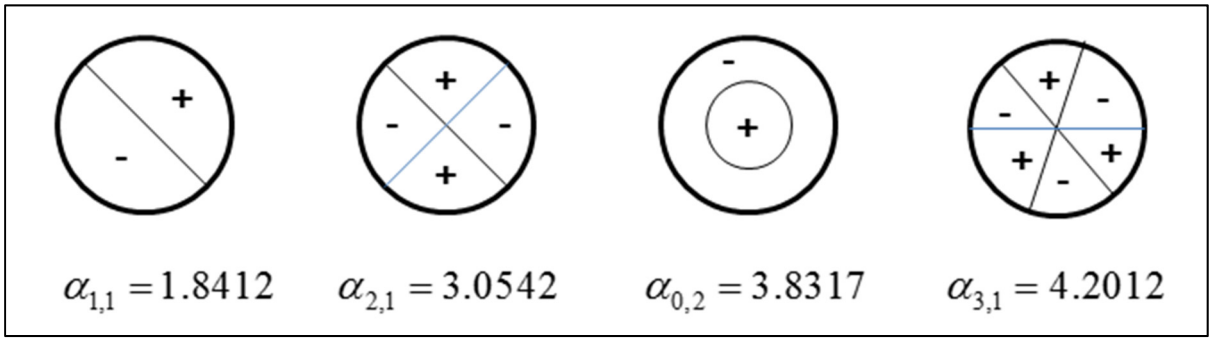

Figure 4 - First four eigenmodes.

In principle, the double infinity of coefficients $C_{n,i}^o$ and $C_{n,i}^b$ can be computed when initial conditions are known. However, describing how the block drops, hits the brine-oil interface and breaks when reaching the bottom of the cavern is beyond our reach here. In fact, oil and brine are viscous, and dampening occurs. After some time, the eigenmodes whose periods are shortest vanish, as they are associated with high-frequency oscillations: dampening is faster when the period is shorter. At the very beginning, the 2-3 first modes can be observed. After some time, from a practical point of view, only the first mode (1,1) is active. A typical shape is drawn on Figure 5. (This shape can be observed when rocking a water-filled plate.)

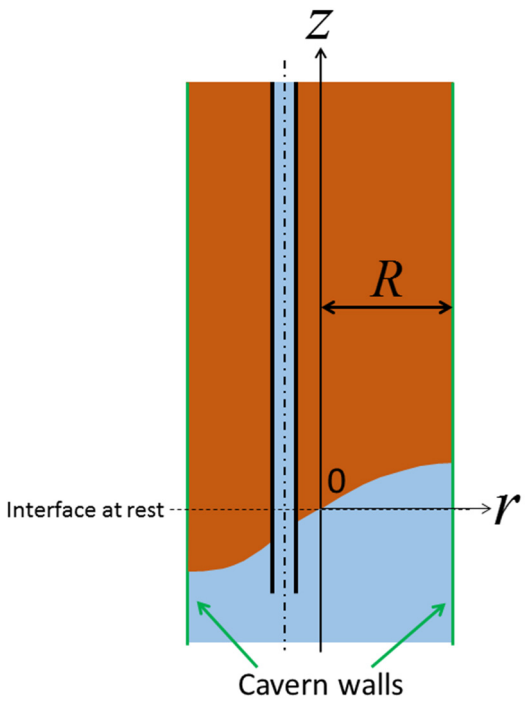

Figure 5 - First eigenmode (1,1), vertical cross-section of the cavern.

Period of the eigenmodes

In many cases, the cavern radius is smaller than brine or oil height: $\alpha_{n,i}h_b/R$ or $\alpha_{n,i}h_o/R$ are much larger than 1 and periods of eigenmodes are

$$T_{n,i} \approx 2\pi\sqrt{\frac{(\gamma_b + \gamma_o)R}{(\gamma_b - \gamma_o)g\alpha_{n,i}}} \tag{5}$$

When $R = 33$ m (110 ft), the two first periods are $T_{1,1} = 20.6$ s and $T_{0,2} = 14$ s. On Figure 2, it is clear that in the BH112B cavern, one minute after block fall, the pressure-oscillation period is 20 seconds. However, immediately after block fall, pressure changes are a combination of several modes, and quarter waves in the wellbore also may play a role. Pressure sampling rate is not fast enough to identify all these modes.

Wave detection

When the first eigenmode (1,1) is considered, pressure *changes* in the brine body can be written

$$\delta p_b = -\gamma_b \frac{\partial \psi_b}{\partial t} = -\gamma_b C\omega_{1,1}\sin(\omega_{1,1}t)\sinh\left(\frac{\alpha_{1,1}h_o}{R}\right)J_1\left(\alpha_{1,1}\frac{r}{R}\right)\cos(\theta)\cosh\left[\frac{\alpha_{1,1}(z+h_b)}{R}\right] \tag{6}$$

where C (in meters) is a constant, $0 < r < R$, $-h_b < z < 0$, the nodal line is $\theta = \pi/2$, and $\alpha_{11} \approx 1.8412$. Pressure changes are maximum at interface depth ($z = 0$) at the cavern wall ($r = R$) on the diameter perpendicular to the nodal line ($\theta = \pi/2$, Figure 6); they are proportional to C:

$$\delta p_b^{\max} = \gamma_b C\omega_{1,1}\sinh\left(\frac{\alpha_{1,1}h_o}{R}\right)J_1(\alpha_{1,1})\cosh\left(\frac{\alpha_{1,1}h_b}{R}\right) \tag{7}$$

and

$$\delta p_b = -\Delta p_b^{\max} \sin\left(\omega_{1,1} t\right) \cos\left(\theta\right) \frac{J_1\left(\alpha_{1,1} \frac{r}{R}\right)}{J_1\left(\alpha_{1,1}\right)} \frac{\cosh\left[\frac{\alpha_{1,1}\left(z+h_b\right)}{R}\right]}{\cosh\left(\frac{\alpha_{1,1} h_b}{R}\right)} \tag{8}$$

Pressure changes are measured at the wellhead of the brine string; they reflect pressure changes at the end of tubing (EOT) depth. In other words, pressure changes are larger (hence, easier to record) when EOT is closer from the cavern wall, closer from the brine-oil interface and farther from the nodal line. The pressure recording method is extremely cost-effective; its main weakness lies in the fact that the EOT must be located conveniently.

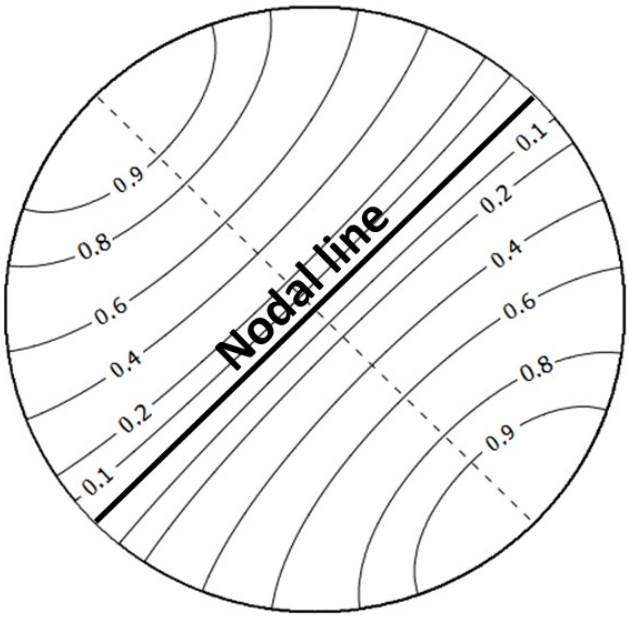

Figure 6 - Relative brine pressure changes ($\delta p_b / \Delta p_b^{\max}$) at interface depth following a salt fall.

Pressure changes and energy

When a salt block whose mass is M (kg) falls by h_f (m) to the bottom of the cavern, potential energy Mgh_f is provided to the fluid-filled cavern. A large part of this energy is lost because of viscous effects. A fraction is converted into kinetic energy as the interface rolls up and down in the cavern. After some time, the kinetic energy contained in the eigenmodes whose periods are shortest has dissipated, and only the first eigenmode is observed. For this reason, it is interesting to compute the relation between the kinetic energy and the amplitude of the pressure changes when the first mode (1,1) is considered: recording pressure changes give an idea of the kinetic energy involved. However, it must be kept in mind that this computed kinetic energy is only a part of total energy Mgh_f that was provided to the system by the block fall.

When $\bar{K}_{1,1}$ is the oil and brine kinetic energy averaged during one period of the first mode, this relation is:

$$\frac{\bar{K}_{1,1}}{\left(\delta p_b^{\max 1,1}\right)^2} = \frac{\pi}{16}\left(\alpha_{1,1}^2 - 1\right)\frac{\left(\gamma_b - \gamma_o\right)Rg^2}{\omega_{1,1}^4 \gamma_b^2 \coth\left(\frac{\alpha_{1,1} h_b}{R}\right)} \tag{9}$$

Conclusion

Following salt falls, pressure fluctuations are observed in oil storage caverns. They are generated by oil-brine interface oscillations. After some time, these oscillations become relatively stable, as the interface rolls up and down in the cavern around a line (nodal line) that experiences no displacement; i.e. the final oil-brine interface depth. These oscillations can be measured at the wellhead. The observed signal strongly depends upon the location of the end of the tubing (EOT) depth below the oil-brine interface. However, the size of the salt block can be determined, especially when the cavern experiences relatively frequent falls.

References

Baar C.A. (1977) - *Applied salt-rock mechanics*. Vol. I. Developments in Geotechnical Engineering. 16-A. Amsterdam: Elsevier Science.

Bérest P., Bergues J., Brouard B. (1999). *Review of static and dynamic compressibility issues relating to deep underground salt caverns*. Int. J. Rock Mech. Min. Sci., 36, 1031-1049.

Cole R. (2002) - *The Long-Term Effects of High Pressure Natural Gas Storage on Salt Caverns*. SMRI Spring Meeting, Banff, Canada, 75-97.

Crotogino F., Mohmeyer K.U, Scharf R. (2001) - *Huntorf CAES: More than 20 Years of Successful Operation*. SMRI Spring Meeting, Orlando, Florida, 351-362.

Hart D., Bettin G., Bellevue B. (2017). *Pressure Trend Analyses for Geophysical and Integrity Investigations*. SMRI Spring Meeting, Albuquerque, New Mexico.

Munson, DE., Ehgartner, B., Bauer, S., Rautman, C., Myers, R. (2004). *Analysis of a salt fall in Big Hill Cavern 103, and a preliminary concept of salt dome structure*. SMRI Spring Meeting, Wichita, KS. 57-72.

Park B.Y., Ehgartner B.L., Lee M.Y., Sobolik S.R. (July 2005). *Three-Dimensional simulation for Big Hill strategic Petroleum Reserve (SPR)*. Sandia Report, SAND 2005-3216.

Renoux P., Fortier E., Maisons C. (2013) Microseismicity induced within Hydrocarbon Storage in Salt Caverns, Manosque, France. Hazard review and event re-location in a 3D velocity model. SMRI Fall Meeting, Avignon, France.

Rokahr R., Staudtmeister K., Zander- Schiebenhöfer D., Johansen J.I. (2007) - *In-situ Test with a Gas Storage Cavern as a Basis for Optimization*. SMRI Spring Meeting, Basel, Switzerland, 84-97.